Sensors and Actuators A 194 (2013) 181–187

Contents lists available at SciVerse ScienceDirect

Sensors and Actuators A: Physical

journal homepage: www.elsevier.com/locate/sna

Fabrication and testing of ISFET based pH sensors for microliter target solutions

Zhuxin Dong[a,*], Uchechukwu C. Wejinya[a], Imad H. Elhajj[b]

[a] Department of Mechanical Engineering, University of Arkansas, Fayetteville, AR 72701, USA
[b] Department of Electrical and Computer Engineering, American University of Beirut, Beirut 1107 2020, Lebanon

ARTICLE INFO

Article history:
Received 7 November 2012
Received in revised form 2 February 2013
Accepted 3 February 2013
Available online 13 February 2013

Keywords:
MEMS
ISFET
pH
Microliter

ABSTRACT

In recent years, there has been an increasing interest in the monitoring and controlling of pH. It has become an important aspect of many industrial wastewater and water quality treatment processes. At the same time, the demand for smaller electronic devices used for various industrial, commercial, and research applications has greatly increased. In this paper, we propose a fabrication method of ion-sensitive field effect transistor (ISFET) using micro–electro-mechanical systems (MEMS) techniques for pH sensing application. The novelty of this device lies in the detection of target solution with volumes in the sub-microliter range. With proper electrical packaging, our ISFET chip has been able to detect the pH values of 2.5 μL solutions. The results reveal a linearity of pH measurement with a corresponding sensitivity of 10.7 mV/pH. Furthermore, Nernst equation is employed to analyze the performance, and a promising scheme to improve the sensitivity while measuring tiny solutions is proposed. This achievement has the potential to satisfy the research demands in various areas including chemistry, biology and medicine.

1. Introduction

Since Bergveld introduced the ion-sensitive field effect transistor (ISFET) in 1970 [1], the sensor industry has expanded rapidly. The concept upon which the ISFET works has a variety of applications, including those in the medical field, food industry, wastewater treatment processes, and soil nutrient analysis [2]. The durability, quick response time, accuracy, and small size of ISFETs make them more advantageous to use than conventional glass electrode pH sensors. Additionally, they are less expensive to manufacture [3]. Because of the widespread use of ISFETs, much attention has been given toward making them smaller, more sensitive, and more efficient. Reducing their size would open new possibilities for incorporating them into smaller electronics such as personal drug monitoring devices [3]. At the same time, smaller devices would allow for the analysis of smaller targets, thereby reducing unnecessary waste of the sample solution.

ISFET based pH sensor is one of the most well-known applications [4,5]. The concept of the ISFET is easily understood by comparing it to a Metal-oxide Semiconductor Field-Effect Transistor (MOSFET) [6]. Although these two devices have the same equivalent circuit, there are still some key differences in their designs. As shown in Fig. 1, a reference electrode and an ion-sensitive membrane in the ISFET take the place of the metal gate in a MOSFET. When a solution contacts the ISFET gate insulator membrane, an ion interaction occurs that results in a voltage being applied to the gate. This ion activity at the solution–membrane interface is described by the Nernst equation. Under the gate voltage, a conducting channel forms between the source and drain, allowing current to flow through the device. As the ion activity at the membrane changes, the gate voltage changes also, and the drain current is a unique function of the gate voltage. Therefore by measuring the change of the gate voltage while adjusting the gate voltage to keep the drain current constant, the ion concentration of the solution can be determined [7].

The objective of this paper is to fabricate ISFET structure in 1.2 mm × 0.7 mm area and obtain the pH measurement sensitivity. The gate area, which is the gap of 40 μm between the source and drain, can be used to contact with target solution in microliter scale. The inversion layer share the same length of 40 μm, which ensures the feasibility that nanochannels can be fabricated to connect the source and drain as Atomic Force Microscopy (AFM) is able to carry out surface nanomachining easily within that size. Through proper MEMS fabrication steps, ISFET chips are produced and tested with microliter scale target solutions from pH 4 to 10. The sensitivity and response time are obtained as well. Furthermore, a mathematical model is built up to analyze the experimental results. According to the comparison between the experimental and theoretical data, we are confident to improve the sensor performance, and we believe bringing some specified nanomaterial

* Corresponding author. Tel.: +1 479 575 4800; fax: +1 479 575 6982.
E-mail address: dzhuxin@uark.edu (Z. Dong).

0924-4247/$ – see front matter © 2013 Elsevier B.V. All rights reserved.
http://dx.doi.org/10.1016/j.sna.2013.02.008

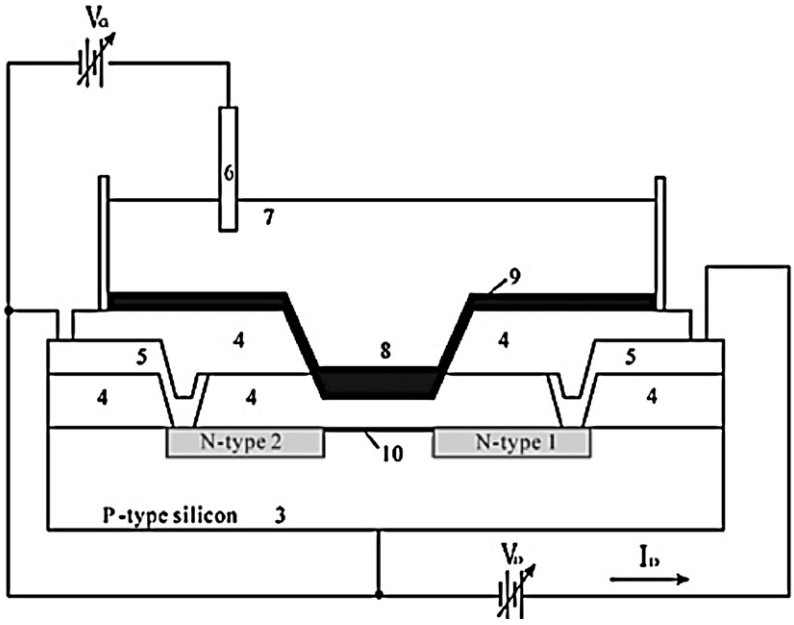

Fig. 1. Schematic diagram of a composite gate, dual dielectric ISFET: 1, drain; 2, source; 3, substrate; 4, insulator; 5, metal contacts; 6, reference electrode; 7, solution; 8, electroactive membrane; 9, encapsulant; and 10, inversion layer.

into our current ISFET structure should be very promising. As a matter of fact, the ISFET chips, which possess the compatibility with nanomaterials, are also designed and included in the same wafer as it will be one of the focuses of our continuous work.

2. Fabrication of ISFET

The fabrication process of our ISFET consists of eight major steps, all of which were completed using the cleanroom thin film facilities in High Density Electronics Center (HiDEC) of University of

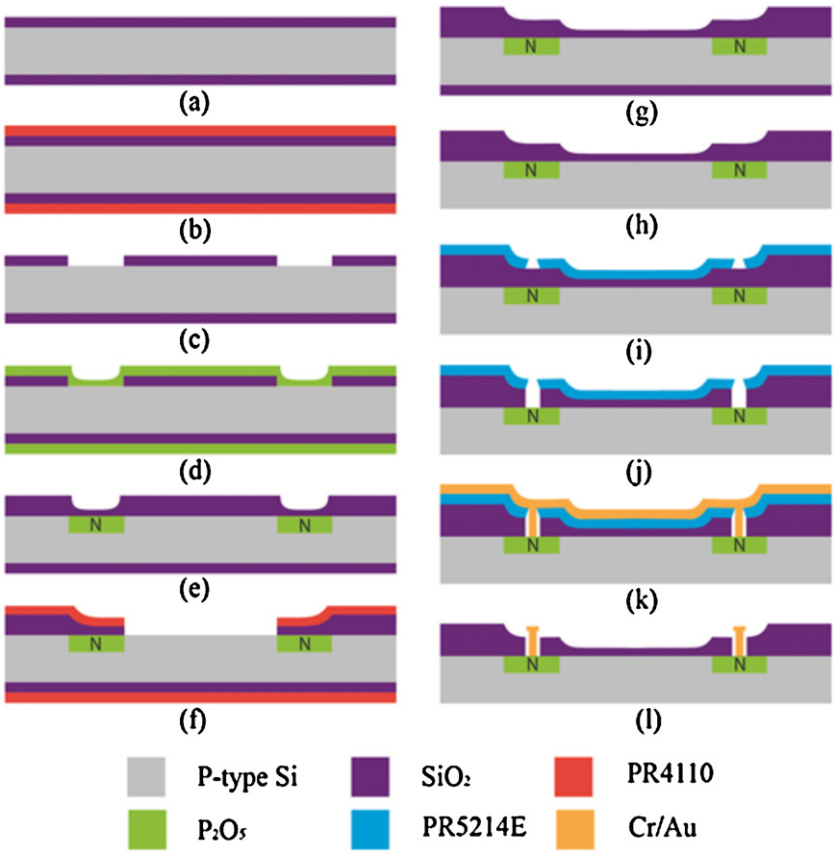

Fig. 2. Diagram of the fabrication of ISFET: (a) oxidation, (b) apply PR, (c) pattern for diffusion, (d) pre-deposition of dopant, (e) dopant drive-in, (f) pattern for gate, (g) gate oxidation, (h) backside oxide etch, (i) lift-off PR pattern, (j) oxide etch on doped area, (k) metal deposition, and (l) lift-off.

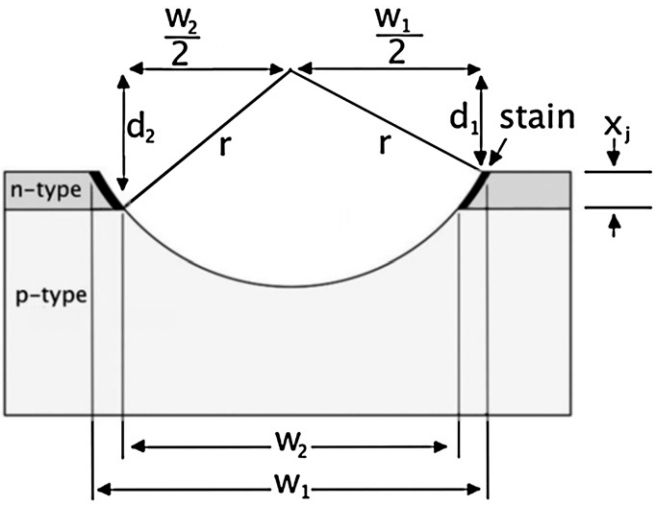

Fig. 3. Junction sectioning geometry.

Arkansas. The fabrication started with a 5-inch p-type boron diffused silicon wafer with orientation of <1 1 1> and thickness of 625 μm. The eight major steps are Field Oxidation, Phosphorus Source Preparation, Pre-Deposition, Drive-in, Gate Oxide, Backside Oxide Etch, Lift-off Photoresist (PR) Patterning, and Metallization as shown in Fig. 2.

2.1. Field oxidation

During the fabrication, a diffusion furnace (Bruce BDF4, Bruce Technologies Inc., USA) was used for oxidation and phosphorus diffusion. The objective of field oxidation is to grow a silicon dioxide layer of about 500 nm thick on the polished side of the wafer. Inside the oxidation tube, the wafer first underwent a Dichloroethylene (DCE) clean at 750 °C. Then, the temperature was increased to 1100 °C to complete dry oxidation and wet oxidation.

2.2. Phosphorus source preparation

The phosphorus source preparation was done in a specific phosphorus tube. The source wafer was a PH-950 n-type 5-inch wafer with active component of SiP_2O_7. The tube was first dried in N_2 at 400 °C for 1 h. Then, the temperature rose to 885 °C, and the temperature stayed at 885 °C for 18 h with N_2 and O_2. Then, the tube temperature was decreased to 400 °C for 1 h. After this process, the tube was filled with the dopant vapor P_2O_5 from the source by direct volatilization.

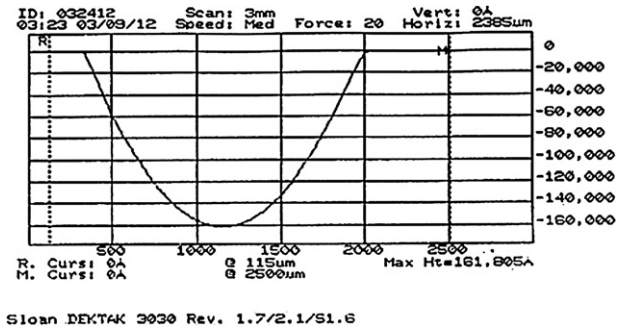

Fig. 4. Groove depth measurement.

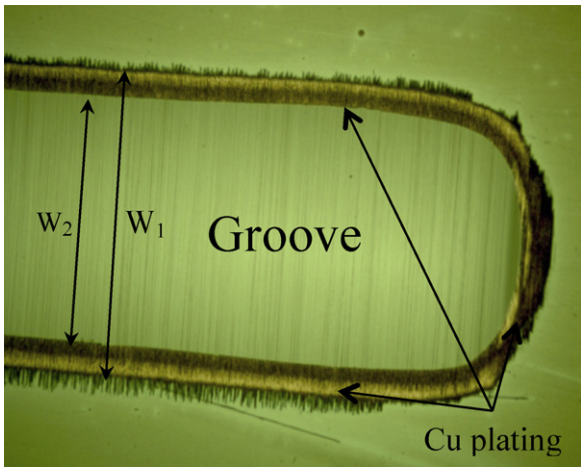

Fig. 5. Inspection (top-view) of Cu plating after junction stain applied on control wafer C1 by optical microscopy.

2.3. Pre-deposition

Photolithography is necessary prior to the pre-deposition process. It was used to pattern desired diffusion areas on the wafer. After proper coating, UV exposure, developing, wet etching and stripping, the wafer was loaded to the phosphorus tube. The deposition begun at 700 °C for 30 min, and then the temperature was increased to 885 °C for 65 min. The deposition ended with another 35 min treatment at 700 °C. Therefore, the wafer was uniformly covered by the dopant. Besides the process wafer, a control wafer C1 was also loaded in this process in order to investigate the diffusion quality. After pre-deposition, the wafers underwent a deglaze process, which was used to remove the excess un-reacted dopant.

2.4. Diffusion drive-in

The dopant deposited on Si diffused in this step by loading the wafers into the phosphorus tube at high temperatures with N_2, O_2, and steam flow. After the drive-in, the diffused areas were covered by a thin SiO_2 layer. The SiO_2 thickness on C1 is supposed to be the same as the one of the diffused areas on the process wafer. Besides measuring the thickness of SiO_2, C1 was also used to calculate the junction depth, for which a groove is needed on the doped silicon surface. The junction sectioning geometry is illustrated in Fig. 3. After removing SiO_2 layer on C1, a groove was fabricated by using a wafer groover. The blade of wafer groover has a radius of 19,885 μm, and the groove depth was 16 μm measured by Dektak 3030 as shown in Fig. 4. A droplet of n-type stain solution was applied to the groove area and exposed by the aligner. Then, the stain was removed by dipping the wafer into DI water and blow-dry with N_2. The copper plating on the doped area was inspected by microscopy as shown in Fig. 5. Next, an optical microscope was employed to determine W_1 and W_2, which were 1692.4 μm and 1442.7 μm respectively. According to the geometry in Fig. 3, the junction depth x_j was able to be calculated using Eq. (1). Ultimately, the junction depth on C1 was obtained, $x_j = 4.9$ μm.

$$x_j = d_2 - d_1 = \sqrt{r_2 - \left(\frac{W_2}{2}\right)^2} - \sqrt{r_2 - \left(\frac{W_1}{2}\right)^2} \quad (1)$$

2.5. Gate oxide

Since the direct contact between target solutions and the transistor happens on the gate area, a fine thin oxide layer is needed instead of the current thick layer. Thus, photolithography was used

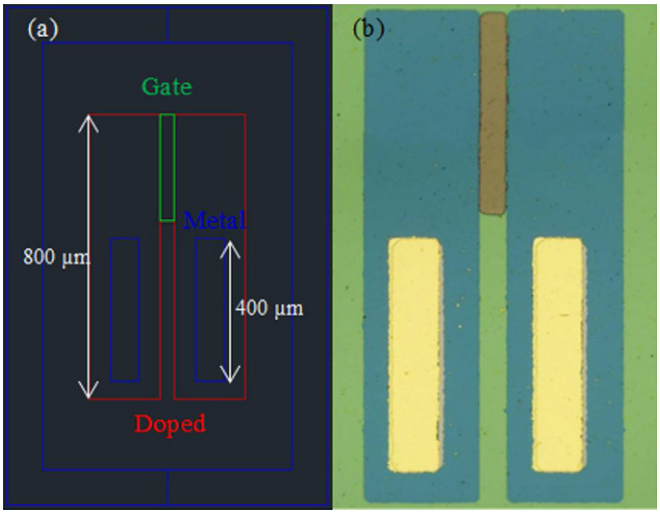

Fig. 6. Structure of ISFET: (a) desired and (b) fabricated.

again to pattern the gate areas. When the SiO_2 layer on the gate areas was removed, the process wafer was ready to go back to the furnace for gate oxidation with a second control wafer C2. Besides DCE clean, the gate oxidation process only involved dry oxidation with O_2. Based on the oxidation thickness measurement through Nanospec microscopy, each gate area has about 560-Å-thick oxidation layer in the process wafer, while the thickness of oxidation layer on the diffused areas is about 1310 Å.

2.6. Backside oxide etch

The frontside of the process wafer was first coated by PR to protect the oxidation layer on the polished side during etching the oxidation off the backside. Then, a flood exposure followed by developing was used to strip off the entire PR.

2.7. Lift-off PR patterning

In order to pattern the metal layer using lift-off, an image reversal (IR) photoresist AZ 5214E [8] was used. After a clearfield mask exposure and a flood exposure to activate its IR mode, the PR was developed using MF CD-26 developer for 45 s. The PR exposed only once was developed, and the corresponding SiO_2 was etched.

2.8. Metallization

Metallization was realized using thermal evaporation (Edwards 306 Turbo). Chromium and gold were deposited onto the process wafer. The chromium as an adhesion layer was 15 nm thick, and the gold layer was about 233.8 nm thick. To lift off the metal, an ultrasonic cleaner was used. The process wafer was put into a crystallizing dish which was filled with acetone. Then the dish was moved into the ultrasonic cleaner and floated on the top of water. The ultrasonic was turned on for 5 min, and the metal started to be lifted off. Hereby, our ISFET chips were completed. Fig. 6 illustrates an example of our fabricated ISFET. The gold layer was about 2000 Å above the SiO_2 layer on the doped area as measured in Fig. 7. More details regarding the fabrication can be found in the supplementary document of this paper.

3. Experimental setup

After cutting the process wafer into pieces of ISFET chip using a dicing saw system (Microautomation Model 1100), a small outline

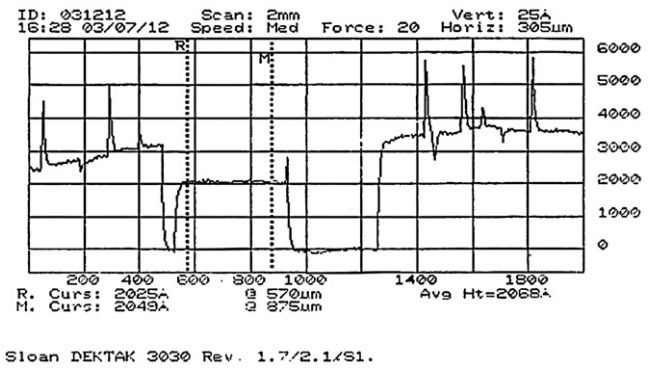

Fig. 7. Metal thickness measurement above the doped area.

integrated circuit package (CSO00802, Spectrum Semiconductor Materials Inc., USA) was employed in order to establish reliable electrical connections, through which outer electronic devices could be applied. Fig. 8(a) shows the schematic of setup. There is a metal layer on top of the package cavity, and the cavity area fits more than two ISFET chips. Two ISFET chips were attached onto the cavity surface by conductive epoxy. Then, as seen in Fig. 8(b), the gold on the doped areas of the two chips and the metal layer on the package cavity were wire-bonded to different pins through a wire bonder (Model 4123, Kulicke & Soffa, Singapore), which provides 25.4 μm diameter aluminum wire bonding. During the pH measurement, this structure employs a discrete null-balancing method and the output of ISFET, drain current I_d, will be held constant by adjusting the gate voltage V_{gs}. When gate area of the ISFET chip is exposed to various target solutions, the external bias voltage V_{gs} in series with the reference electrode should be adjusted to secure zero change of I_d. Therefore, the change of V_{gs} depends directly on the ionic activity/concentration. In this experiment, the drain voltage V_{ds} was constant at 1 V provided by a DC power supply (Model XP-760, Elenco Electronics Inc., USA), and I_d is measured by a picoammeter (Model 6485, Keithley, USA). A second DC power supply (Model N5748A, Agilent, USA) with a fine adjustable function at 0.01 V was employed to adjust V_{gs}. A copper wire in diameter of 250 μm (Model 93-2972, Strem Chemicals, USA) was used to detect target solutions. Thus, our ISFET is ready for measuring pH of any target solution.

4. Current results

Before testing, six target solutions were prepared. Their pH values were calibrated using a pH tester (pH55, Milwaukee Instruments, USA) and were 4.1, 5, 6, 7.1, 8.5, and 9.5 respectively. In order to test the ISFET, five droplets of 2.5 μL from each target solution were dropped onto the gate area by a pipette and measured. For instance, a droplet from pH 4.1 solution was located onto the gate area using a pipette while the drain voltage was applied at 1 V. Then, the reference electrode was inserted into the droplet while the gate voltage was applied and adjusted to keep the drain current constant at 5.475 mA. When the drain current was stabilized, the gate voltage was recorded. The droplet will evaporate quickly after the gate voltage is applied. Thus, the reading resumed after a short time interval for the same solution until five experimental data are recorded. Then, the ISFET chip was stored overnight in a dry box (McDry MCU-201, Seika Machinery Inc., USA), where the relative humidity is as low as 1 percent in order to eliminate the effect of the evaporation of previous solutions. Then, the measurement for next pH solution could be carried out the next day. The entire experiment was carried out in a cleanroom lab where the room temperature always remained constant and a thermometer

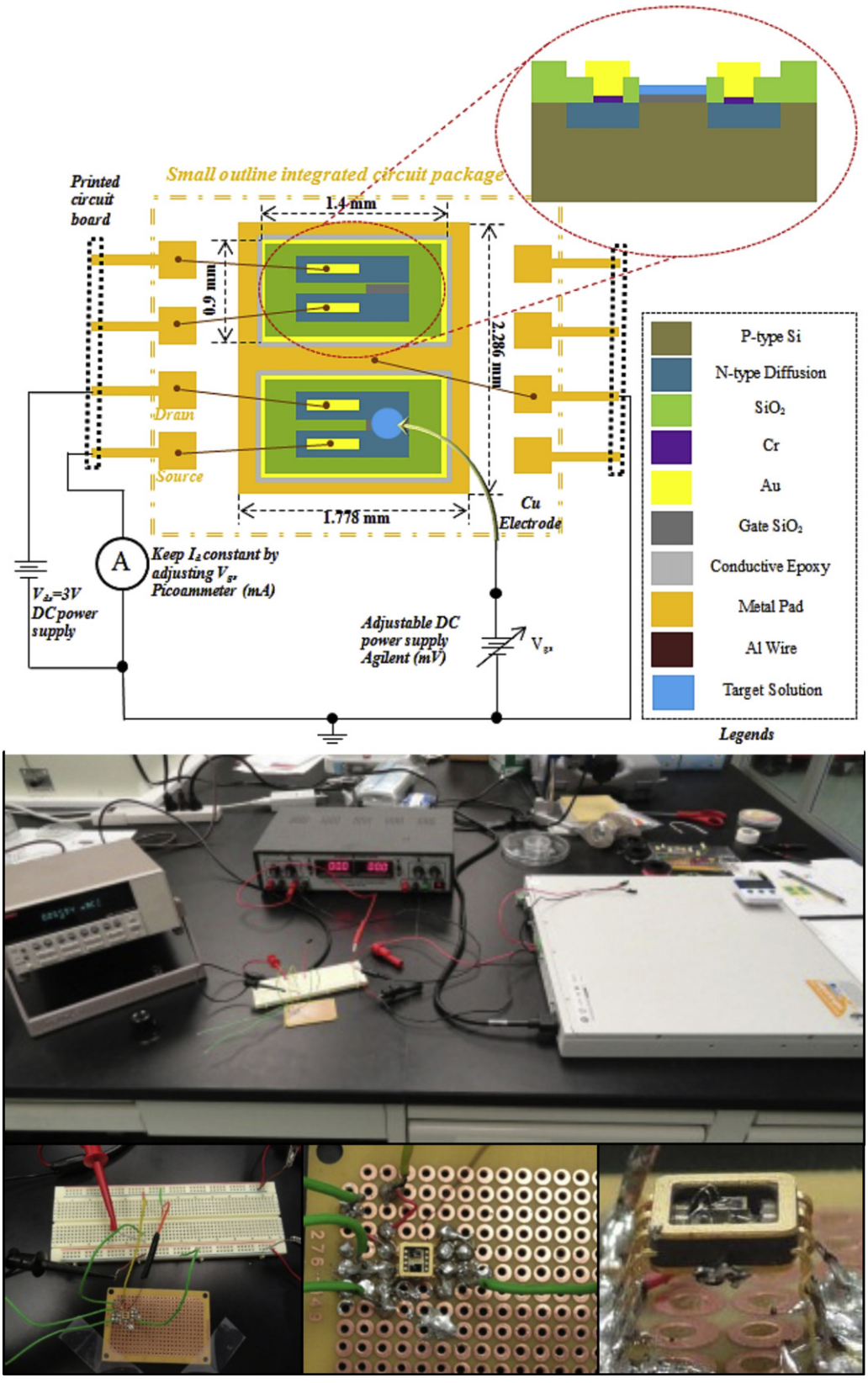

Fig. 8. Experimental setup for pH measurement: (a) schematic and (b) real.

is used to monitor it. Otherwise, the variation of ambient temperature will greatly influence the pH measurements. Eventually, the complete results for pH detections between 4.1 and 9.5 were given in Table 1. Furthermore, the corresponding ΔV_{gs} at each pH was collected to apply a linear fit in order to study the sensitivity of the ISFET as shown in Fig. 9. According to the linear fit, the slope is 0.0107, which means the sensitivity is 10.7 mV/pH. Additionally, the ISFET had an instant response. Once a steady contact between

Table 1
Results of pH measurement using ISFET.

pH	V_{gs} (V)							
	#1	#2	#3	#4	#5	Mean	Std. dev.	ΔV_{gs}
4.1	0.52	0.51	0.5	0.53	0.53	0.518	0.01304	−0.042
5	0.54	0.54	0.56	0.56	0.56	0.552	0.01095	−0.008
6	0.56	0.57	0.56	0.57	0.56	0.564	0.00548	0.004
7.1	0.56	0.56	0.55	0.57	0.56	0.56	0.00707	0
8.5	0.58	0.58	0.59	0.58	0.57	0.58	0.00707	0.02
9.5	0.6	0.59	0.58	0.58	0.58	0.586	0.00894	0.026

The entire measurement was completed under consistent conditions: V_{ds} = 1 V and I_d = 5.475 mA.

the electrode and the solution is made, there is an instant change in the drain current I_d. Then, the gate voltage V_{gs} is adjusted to maintain the current constant at 5.475 mA, which takes less time hence we have enough time to finish the experiment.

5. Modeling analysis–Nernst potential

As known, pH is defined as the decimal logarithm of the reciprocal of the hydrogen ion activity a_{H+} in a solution as in Eq. (2). As a matter of fact, hydrogen ion activity is always approximated to the free hydrogen ion concentration [H⁺]. Thus, we can use Eq. (3) to describe the definition of pH in solution instead. Furthermore, the pH measurement using ISFET is based on the principle of Nernst potential, which has a physiological application when it is used to determine the potential of an ion of charge z across a membrane. This potential is calculated using the concentration of the ion both inside and outside the cell. Eq. (4) expresses the meaning of the Nernst potential, where E is the Nernst potential in voltage, R is the ideal gas constant in joules per kelvin per mole, T the is temperature in kelvin, F is the Faraday's constant in coulombs per mole, z is the valence of the ion (z = 1 for hydrogen ion), and $[H_1{}^+]$ and $[H_2{}^+]$ are the hydrogen ion concentration outside cell and inside cell respectively, which, in our case, are the ion activity I_d and the hydrogen ion concentration in the target solution. Therefore, if the ion activity/concentration in either side of the membrane is kept constant, the Nernst potential only depends on the ion activity/concentration in the other side of the membrane and the Nernst potential can be used as output to reflect the ion activity/concentration of target solution. In the experiment, both I_d and V_{ds} are held constant during the pH measurement while the measured potential V_{gs} indicates the pH of the target solution. Eqs. (5) and (6) reveal the relation between the measured Nernst potential and the pH, where E^0 is the standard membrane potential at the temperature of interest and a constant due to constant I_d and V_{ds}.

$$\mathrm{pH} = -\log_{10}(a_{H^+}) = \log_{10}\left(\frac{1}{a_H}\right) \tag{2}$$

$$\mathrm{pH} = -\log_{10}(H^+) = \log_{10}\left(\frac{1}{H^+}\right) \tag{3}$$

$$E = \frac{RT}{zF}\ln\left(\frac{a_{1H^+}}{a_{2H^+}}\right) = 2.303\frac{RT}{zF}\log_{10}\left(\frac{[H_1^+]}{[H_2^+]}\right) \tag{4}$$

$$E = \frac{RT}{zF}(\log_{10}[H_1^+] - \log_{10}[H_2^+]) = E^0 - 2.303\frac{RT}{zF}\log_{10}[H_2^+] \tag{5}$$

$$E = E^0 + 2.303\frac{RT}{zF}\mathrm{pH} \tag{6}$$

$$E = E^0 + 059172\mathrm{pH} \tag{7}$$

After substituting the constants, $R = 8.314472\,\mathrm{JK^{-1}\,mol^{-1}}$, T at room temperature 25 °C which is 298.16 K, z = 1 and $F = 96{,}485.3\,\mathrm{C\,mol^{-1}}$, Eq. (6) is rewritten as in Eq. (7). As we can see, the slope of the relation between Nernst potential and the pH of target solution is 0.059172 V/pH or 59.2 mV/pH. Apparently, the Nernst equation is a mathematical description of an ideal pH electrode behavior. Therefore, the slope of 59.2 mV/pH is an ideal sensitivity of ISFET based pH sensor when pH is measured by the means of Nernst potential. Fig. 9 also presents the comparison between the pH sensitivity of current ISFET and the ideal Nernst slope.

One of the major factors that cause a low sensitivity in the current pH measurement is the volume of target solution is scaled down to microliter while conventional pH sensors generally require the target solution in at least milliliter scale. As shown in Fig. 10 [9], the quantity of ions decreases significantly while the volume is reduced even if the corresponding concentration is kept the same. A small change of the concentration of solvated hydrogen ion in a huge solution would bring a great number of more/less ions while a big change of the concentration in a tiny solution would produce a little more/less ions, which is why there is a relatively lower sensitivity of pH when the solution volume is largely decreased. To measure the pH value for solutions in microliter or molecule level is one of the significant novelties for this project. However, the sensitivity has to be affected owing to the largely reduced volumes. It has been reported that an ISFET fabricated similarly but with extra p-type stop channel using boron diffusion reached a

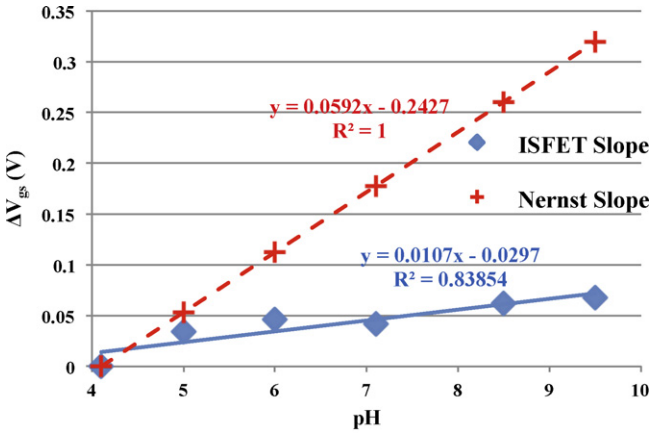

Fig. 9. Current pH sensitivity of our ISFET vs. ideal Nernst slope.

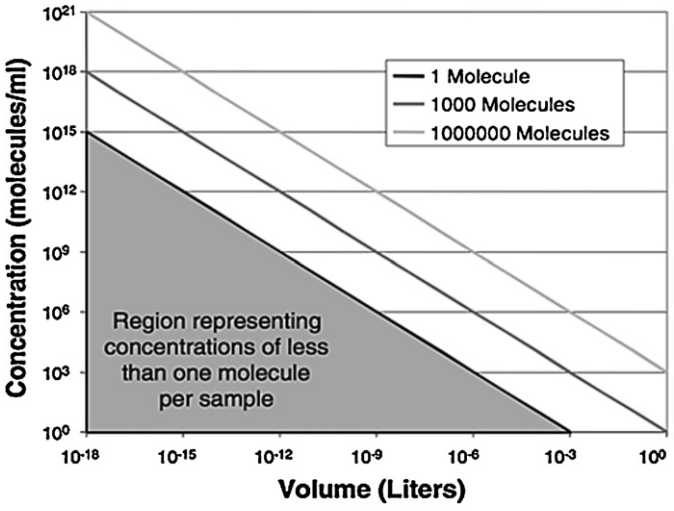

Fig. 10. Relation between quantity of molecules and volume/concentration [9].

sensitivity of 40 mV/pH [7]. Their ISFET device was also equipped with an optimized reference electrode. However, the device was totally immersed into the target solution for measuring pH, which means relatively large volume of target solution was necessary to reach the sensitivity. Furthermore, it was mentioned in [10] that a layer of silicon nitride on the top of gate oxide as the ion sensing material might be able to improve the ISFET performance. Unfortunately, so far it has not been reported any research work regarding an effective compensation for measuring solutions in microliter or molecule level. However, we have proposed Carbon Nanotube (CNT) integrated ISFET as a potential solution [11]. In the future, a bundle of CNTs will be aligned in the nanochannel by the means of Dielectrophoresis (DEP) in order to seek an improved performance. AFM based nanoscratching for nanochannels on Si substrate with a diamond tip [12] and CNT alignment using DEP [11] have been proved feasible by our previous work. Therefore, CNTs integrated ISFET is proposed as a promising scheme to improve the sensor performance while it is used to measure microliter solution targets due to CNTs' remarkable electrical properties, such as high current carrying capacity (CNTs: $\sim$1 TA/cm^3 vs. Cu 1 GA/cm^3), which could be a significant contribution for applications in various areas, including medicine, biology, chemistry, medicine and industry.

6. Conclusion

ISFET chips have been successfully fabricated based on a 5-in-diameter p-type silicon wafer using MEMS fabrication techniques. N-type phosphorus dopants are diffused into the wafer to form the source and drain areas for each ISFET structure. The junction depth is measured, and the diffusion is verified. In addition, photolithography, evaporation, and lift-off techniques are involved during the fabrication. With a proper method of packaging, one of the ISFET chips has been tested as a pH sensor. The testing samples from six different solutions with pH values from 4.1 to 9.5 are as small as 2.5 μL. The experimental results indicate a linearity of pH measurement with a corresponding sensitivity of 10.7 mV/pH. In addition, according to the mathematical modeling analysis, there is a huge potential to improve the current sensitivity of our ISFET chip as a pH sensor for microliter scale solution targets. Furthermore, we have proposed that CNTs are able to be integrated to ISFET using AFM in order to improve its performance significantly.

Ongoing research has been focusing on the fabrication of ISFET chip in various dimensions, and CNTs will be embedded into the system using AFM-based nanoscratching during the fabrication procedures.

Appendix A. Supplementary data

Supplementary data associated with this article can be found, in the online version, at http://dx.doi.org/10.1016/j.sna.2013.02.008.

References

[1] P. Bergveld, Development of an ion-sensitive solid-state device for neurophysiological measurements, IEEE Transactions on Biomedical Engineering BM17 (1970) 70.
[2] C. Jimenez-Jorquera, ISFET based microsensors for environmental monitoring, Sensors 10 (2010) 61–83.
[3] C. Lee, Ion-sensitive field-effect transistor for biological sensing, Sensors 9 (2009) 7111–7131.
[4] P. Bergveld, Thirty years of ISFETOLOGY what happened in the past 30 years and what may happen in the next 30 years, Sensors and Actuators B 88 (2003) 1–20.
[5] P. Bergveld, ISFET, theory and practice, in: Proceedings of IEEE Sensor Conference, Toronto, October, pp. 26, 2003.
[6] H.C. Casey Jr., Devices for Integrated Circuits-Si and III-V Compound Semiconductors, John Wiley & Sons, Inc., New York City, 1999, Chapter 8, pp. 342–426.
[7] S.C. Chen, Y.-K. Su, J.S. Tzeng, The fabrication and characterization of ion-sensitive field effect transistors with a silicon dioxide gate, Journal of Physics D: Applied Physics 19 (1986) 1951–1956.
[8] Product data sheet of photoresist AZ 5214E. Available: http://groups.mrl.uiuc.edu/dvh/pdf/AZ5214E.pdf
[9] W.J. Jack, Microelectromechanical systems (MEMS): fabrication, design and applications, Smart Materials and Structures 10 (2001), pp. 1115.
[10] U. Hashim, M.K. Md Arshad, C.S. Fatt, Silicon nitride gate ISFET fabrication based on four mask layers using standard MOSFET technology, in: Proceedings of IEEE International Conference on Semiconductor Electronics (ICSE), Johor Bahru, Malaysia, November 25–27, 2008.
[11] Z. Dong, U.C. Wejinya, S.N.S. Chalamalasetty, Development of CNT-ISFET based pH sensing system using atomic force microscopy, Sensors and Actuators: A. Physical 173 (2012) 293–301.
[12] D. Zhuxin, C. Uchechukwu, Wejinya atomic force microscopy based repeatable surface nanomachining for nanochannels on silicon substrate, Applied Surface Science 258 (2012) 8689–8695.